ASME Journal of Mechanical Design
Online journal at:
https://asmedigitalcollection.asme.org/mechanicaldesign

A Disassembly Scoring Framework for Human–Robot Collaboration Based on Robotic Capabilities

Hao-Yu Liao
Environmental Engineering Sciences,
University of Florida,
Gainesville, FL 32611
e-mail: haoyuliao@ufl.edu

Terrin Pulikottil
Department of Mechanical Engineering,
KU Leuven, Flanders Make@KU Leuven,
Leuven 3000, Belgium
e-mail: terrin.pulikottil@kuleuven.be

Jef R. Peeters
Department of Mechanical Engineering,
KU Leuven, Flanders Make@KU Leuven,
Leuven 3000, Belgium
e-mail: jef.peeters@kuleuven.be

Sara Behdad[1]
Environmental Engineering Sciences,
University of Florida,
Gainesville, FL 32611
e-mail: sarabehdad@ufl.edu

Product disassembly is integral to remanufacturing and recovery operations of end-of-use devices. Traditionally, disassembly has been conducted manually with significant safety risks to human workers. In recent years, robotic disassembly has gained popularity to alleviate human workload and safety concerns. Despite these advancements, robots have limited capabilities in handling all disassembly tasks independently. It is essential to assess whether a robot is capable of performing specific disassembly tasks or not. This study proposes a disassembly scoring framework that evaluates robotic feasibility for disassembling components based on five design-related factors: weight, shape, size, accessibility, and positioning. For each factor, a disassembly score is defined to analyze its specific impact on robotic grasping and placement capabilities. Further, the relationship between the five factors and robotic capabilities, such as grasping and placing, is discussed by an example of the UR5e manipulator. To show the potential for automating the generation of disassembly metric, the Multi-Axis Vision Transformer (MaxViT) model is used to determine component sizes through image processing of the XPS 8700 desktop. Moreover, the application of the proposed disassembly scoring framework is discussed in terms of determining the appropriate work setting for disassembly operations under three main categories: human–robot collaboration (HRC), Semi-HRC, and Worker-Only settings. A disassembly time metric for calculating disassembly time for HRC is also proposed. The study outcomes determine the proper work settings based on the robotic capability.
[DOI: 10.1115/1.4068476]

Keywords: disassembly score, ease of disassembly, human–robot collaboration, machine learning, automated rating systems, remanufacturing, design for disassembly, design for the environment, robotic systems

1 Introduction

Disassembly is essential for breaking down used products, such as electronic waste (e-waste) for end-of-use recovery. The increasing rate of e-waste generation creates significant environmental and health risks due to the improper disposal and management of toxic materials in discarded electronics. Disassembly mitigates the risk of e-waste landfilling by extending the product lifecycle through repair, remanufacturing, and recycling. Integrating robotics and optimizing disassembly sequences diminish the labor-intensive nature of disassembly and improves the economic viability of remanufacturing [1,2].

The design for end-of-life recovery efforts is often overlooked in the literature [3], with limited studies on extending product lifespan and reuse [4]. A more integrated approach between the remanufacturing process and product design is becoming increasingly necessary [5]. The problem is particularly acute in automated remanufacturing and robotic disassembly. Implementing strategies such as design for disassembly and design for remanufacturing can facilitate this integration by simplifying operations. For example, modular design [6] reduces the number and complexity of connectors and improves component accessibility.

Previous literature has tried to develop disassemblability score [7] and ease of disassembly metric (eDiM) [8] to determine the feasibility of disassembly of a specific design; however, the assumption is that disassembly is performed manually. These metrics determine how difficult it is for human workers to disassemble a product. Table 1 summarizes several existing metrics relevant to disassembly. The iFixit score [9] and assessment matrix for ease of repair (AsMeR) [10] consider disassembly difficulty as one factor in determining ease of repair. Priority replacement index (PRI) is developed to make decisions on component replacement, while the eDiM [14] and disassemblability [15] specifically focus on evaluating disassembly difficulties. The eDiM is a standard

[1]Corresponding author.

Contributed by the Design for Manufacturing Committee of ASME for publication in the Journal of Mechanical Design. Manuscript received September 15, 2024; final manuscript received April 14, 2025; published online April 30, 2025. Assoc. Editor: Zhenghui Sha.

Table 1 Examples of relevant disassembly scores

Methods	References
Repair metrics such as iFixit score and AsMeR	[9,10]
Replacement metrics such as PRI	[11]
Disassembly metrics such as eDiM and disassemblability	[12,13]

method considering six factors: tool change, identifying connectors, product manipulation, positioning action, fastener disconnection, and removal of unfastened components [8,14]. These scores have a wide range of applications, particularly when evaluating different design alternatives and design-for-X methods [16].

Previous studies have emphasized the importance of considering disassemblability. Disassemblability is among the most significant aspects of design since disassembly is integral to numerous recovery operations such as reuse and repair [15] or end-of-use recovery [17]. Disassemblability is a fundamental consideration in product design [18], as design improvements can facilitate the feasibility of product reuse [19]. It is best practice to consider disassemblability throughout the entire product lifecycle rather than limiting it to component analysis for maintenance [13]. Given existing technologies, this includes the need for the remanufacturing and recycling industry to harvest materials feasibly. Disassemblability indicates the complexity of disassembly operations and the associated costs [20]. A quantitative evaluation metric for disassemblability is a factor that reflects product quality and design features [21].

In recent years, human–robot collaboration (HRC) and robotic-assisted disassembly have become popular due to the potential for reducing human fatigue [22] and removing hazardous materials [23]. Disassemblability can determine whether or not the robot can complete the specific disassembly task[24]. Although previous studies have discussed disassembly scores, the disassemblability score that considers the capabilities of robots is still a research gap. Nonetheless, such a disassembly score would be a practical source for design improvements to assess product circularity and facilitate initiatives such as right-to-repair in Industry 4.0.

This study develops a disassembly score from the robotic aspect. The score determines how easily robots can dismantle a component. The proposed disassembly score is the relationship between the product design features and robot capabilities. Five factors, including component size, shape, weight, accessibility, and positioning, have been considered. The impact of these factors on robotic capabilities, such as grasping and placing, has been further discussed. Finally, the proper work setting (e.g., HRC, Semi-HRC, and Worker-Only) is decided based on the disassembly score to show how the proposed disassembly score can be used in practice. Moreover, the disassembly time of the human worker and the robot is discussed. The Multi-Axis Vision Transformer (MaxViT) machine-learning model is applied to identify the component size using detailed segmented images to automate the process of developing such scores. The proposed disassembly score considers the capabilities of robots rather than human operators. Scores listed in Table 1 focus on humans as the main users of the device. For example, AsMeR assesses manual repair support, PRI incorporates factors such as technological obsolescence, and eDiM evaluates the types of tools operators utilize.

The remainder of this article is organized as follows. Section 2 discusses the methodology for developing the proposed disassembly score. Section 3 discusses a case study to demonstrate the application of the proposed disassembly score. Section 4 discusses the results, and Sec. 5 concludes the article.

2 Methodology

This section discusses the process of developing the disassembly score, the factors considered, and how it can be automated by applying a machine-learning model for competent size classification as one of the disassembly factors.

2.1 Disassembly Scores. The disassembly scoring framework is designed to assess whether robots can perform specific disassembly tasks within a multicomponent product well. Each score evaluates the feasibility of separating components based on the complexity of the component involved. The disassembly score first evaluates various component-specific features, namely size, shape, weight, accessibility, and positioning. Then, it calculates robotic capabilities in grasping and placing to determine the most suitable mode of disassembly. Figure 1 shows the relationship between the five factors, robotic capability, and work settings.

Figure 1 identifies five design factors that impact disassemblability: component size, component weight, component shape, positioning, and accessibility. These factors are directly tied to the product design and are important in determining how easily a robot can disassemble it. To quantify the robotic disassembly capability, the proposed score assesses the impact of these factors in supporting two main functions of robotic grippers: grasping and placing. In addition, the proper work setting is inferred from evaluating these functions.

2.1.1 Disassemblability Factors. Table 2 shows the five factors, each with three categories, with the corresponding score for each category ranging from 1, 3, to 5. A higher score means the robot better handles the object. For example, if the component size is small, the score is 1.

Component size and component weight depend on robotic capability. While some robots are designed for heavy lifting, there is an upper limit to the weight they can handle. Also, robots have size constraints. Robots designed for specific tasks may not be able to handle objects significantly larger or smaller than those they are programmed to work with. The size and weight limits are defined based on 33% and 66% of robotic capability. We reference the work of Parsa and Saadar [20], which proposes a framework for disassembly planning by defining fixed ranges for component size and weight, such as 2, 3.5, and 4 for size and 2, 2.2, and 2.4 for weight. We assume a positive linear relationship exists between the difficulty of robotic disassembly tasks and the characteristics of the components, such as size and weight. As these dimensions increase, the complexity of the tasks for robots also rises.

The focus is mainly on the physical attributes of the components, such as size, weight, shape, and positioning, which significantly influence the ease of disassembly. Also, the accessibility of these components, determined by whether the robotic arm and gripper can reach the disassembly unit, is important. Oversized components may limit robotic performance; too small components can affect the precision with which robots handle tasks. Variations in component weight also require robots to adjust their handling techniques, particularly for heavier components. More geometrically favorable shapes, such as symmetry and regular positioning, generally increase robotic performance. Adequate space around the disassembly object also improves the robot's ability to access and manipulate components. It is essential to consider these five factors as they directly impact robotic performance.

The component shape is defined by reflective symmetric using the following equation [25]:

$$\text{Symmertic value} = 1 - \frac{A_d}{A_L} \tag{1}$$

Upon identifying the axis of symmetry, two regions are evaluated. The larger region donates as A_L and is contrasted with the smaller one to determine the disparity in their areas, represented as A_d. A value of $A_d = 0$ indicates no discrepancy between the two regions, showing a symmetrical shape.

The positioning is determined based on the rotational symmetry (RS). The categorization of objects based on RS order facilitates their classification in terms of ease of manipulation. RS is known by a shape's ability to maintain symmetry upon rotation. The degree of rotation required to achieve this symmetry is referred to as the order of RS [26]. Specifically, objects with an even RS

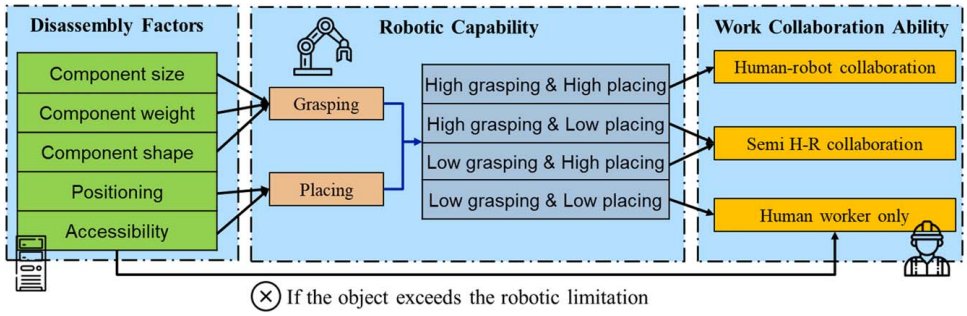

Fig. 1 The relationship between disassembly factors, robotic capability, and work settings

Table 2 The disassembly factors, scores, and the corresponding criteria

Factors	Scores	Criteria
Component size	Large (5)	>56.7 mm and <85 mm
	Medium (3)	>28.3 mm and <56.7 mm
	Small (1)	<28.3 mm
Component weight	Light (5)	<1.67 kg
	Medium (3)	>1.67 kg and <3.33 kg
	Heavy (1)	3.33 kg and <5 kg
Component shape	Symmetric (5)	1
	Semisymmetric (3)	≥0.5
	Asymmetric (1)	<0.5
Positioning	Ease to grasp (5)	Square or RS order of 2, 4, 6
	Moderate to grasp (3)	Cycle or RS order is an odd number or greater than 6
	Difficult to grasp (1)	The RS order is 1 (no rotational symmetry) and no line is parallel
Accessibility	High (5)	Accessible without removing any components
	Medium (3)	Accessible by removing one component
	Limited (1)	Removing more than two obstacles or no space for the gripper

order are considered easy to grasp. On the other hand, objects with an odd RS order, cyclical shapes, or an RS order that exceeds six present moderate difficulty for grasping. An RS order of one indicates the absence of rotational symmetry and the challenge of robotic handling. The RS differs from the axis of symmetry, which can significantly impact the disassembly process. Objects may exhibit low positioning but have symmetrical shapes. For example, the equilateral triangle and the kite are symmetrical but differ in RS, having three and one RS order respectively. Using only RS without considering the axis of symmetry may lead to underestimating the robot's capabilities. For example, rectangles and parallelograms have the same second-order RS, but their shapes differ: rectangles are symmetrical, whereas parallelograms are only semisymmetrical. Therefore, a more complete evaluation of robotic capability requires considering both RS and the axis of symmetry. This concept is illustrated in Fig. 2. Furthermore, accessibility is determined by the number of components that should be removed to access the current component, which depends on the robotic gripper's size. Adequate space is needed so that the robot can quickly grasp the object.

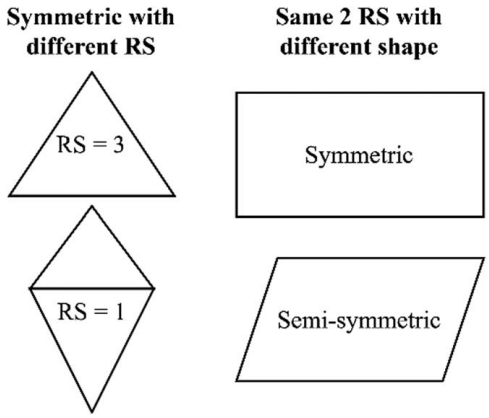

Fig. 2 Illustration of the difference between the axis of symmetry and RS in objects with identical shapes and RS orders

2.1.2 Robotic Capability. In this study, the UR5e robot, equipped with a Robotiq gripper, is used to show the application of the proposed disassembly score. The UR5e's specifications, as listed in the manual, include a maximum payload capacity of 5 kg and a gripper opening of up to 8.5 cm. Based on these specifications, disassembly factors such as component size and weight are categorized into two thresholds, 33% and 66% of the robot's capability, as summarized in Table 2. We should note that the criteria for disassembly score can vary with the type of robotic arm used. We used a two-fingered gripper, while alternative gripper types, such as vacuum or humanoid hand grippers, can be used. In addition, the gripper's maximum length of 15.2 cm is a critical factor for assessing accessibility, as described in Fig. 3. This study uses the UR5e robotic arm to demonstrate the proposed disassembly scores calculations by considering its maximum payload of 5 kg and a gripper opening limit of 8.5 cm. To apply this method to various robotic arms and grippers, payload and gripper opening width parameters should be adjusted to accommodate different robot specifications.

The UR5e robotic arm conducts two main functions: positioning the gripper at designated locations and grasping objects. The performance of the grasping function is impacted by component size, weight, and shape, whereas the positioning function is determined by the factors of positioning and accessibility, as shown in Table 3. Each factor is assigned a median score of 3. The aggregate

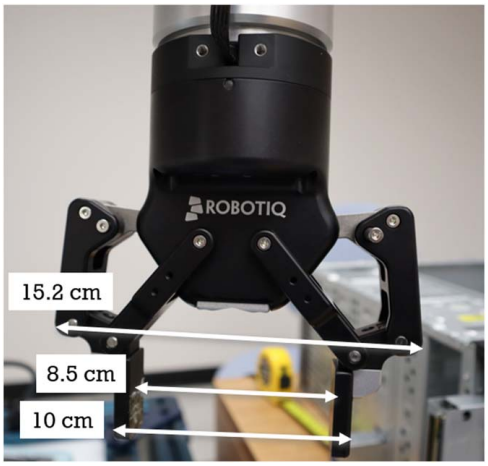

Fig. 3 Robotiq gripper connected with the UR5e

Table 3 The relationship between factors of disassembly scores and robotic capability

Factors	Robotic capability	Scores
Component size	Grasping	Low: ≤9
Component weight		High: >9
Component shape		
Positioning	Placing	Low: ≤6
Accessibility		High: >6

scores of 9 and 6 represent the sum of factors associated with robotic capability and can be benchmarked to distinguish between low and high capability levels.

2.1.3 The Usage of the Disassembly Scoring Framework. The robot's capability determines the work environment configurations, such as HRC, Semi-HRC, and Worker-Only settings, as shown in Fig. 4. In an HRC setting, there is a collaboration between the human worker and the robotic arm, where humans and robots work on the same task. On the other hand, Semi-HRC shows a work setting where tasks between humans and robots are either sequential or parallel. The Worker-Only setting applies when the object's weight or size exceeds the robotic arm's capacity for manipulation and requires direct human intervention without the robot's assistance.

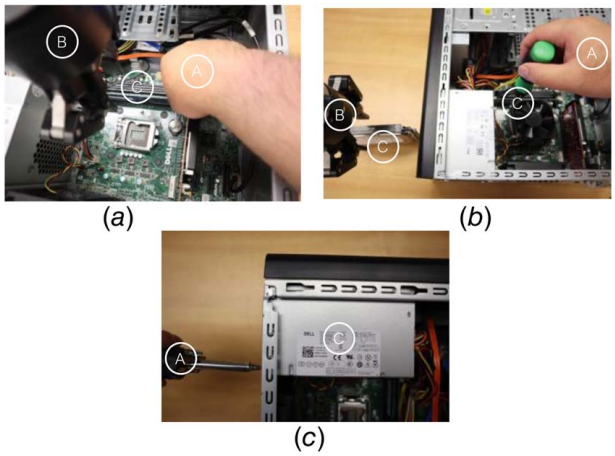

Fig. 4 Comparison of three work settings: (*a*) HRC: a human worker and a robot collaborate directly on the same object, (*b*) Semi-HRC: a human worker and a robot simultaneously work on separate objects, both of which are within the robot's capability for disassembly, and (c) Worker-Only: a human worker alone handles an object that is beyond the robot's capability. In this figure, "A" represents the human worker, "B" the robot, and "C" the disassembly object.

Figure 4 presents three scenarios: (*a*) HRC, (*b*) Semi-HRC, and (*c*) Worker-Only. In Fig. 4(*a*), a human worker and a robot collaborate to disassemble a RAM module. The human releases the slot and holds the RAM while the robot places and grasps it. Figure 4(*b*) depicts Semi-HRC, where the robot grasps the HDD, and the human worker unscrews the CPU fan bolts. The HDD placement follows a sequence where the human disassembles it before the robot intervenes. Figure 4(*c*) illustrates the Worker-Only disassembly of the power supply, as its size prevents the robot from handling it.

2.2 Applying MaxViT to Classify Component Size. The MaxViT machine-learning model is used to determine the size of components, which is a critical factor in disassembly processes. According to Ref. [27], the MaxViT was introduced in 2022. This architecture combines the MaxViT block with Mobile Inverted Bottleneck Convolution (MBConv) [28], Block Attention, and Grid Attention mechanisms. MBConv combines the squeeze-and-excitation module with convolution layers to improve feature extraction. This research uses the MaxViT model to classify component sizes into four categories: small, medium, large, and oversized. The process consists of segmenting the input from an RGB image and categorizing it into one of these four size classes.

2.3 Human–Robot Collaborative Disassembly Time. In practical applications, it is important to note that the allocation of disassembly tasks between humans and robots should be determined based on their capabilities and the disassembly time required for each task. This section introduces a general framework to calculate disassembly times for manual operations and HRC scenarios. We identify the optimal option as the minimum between the manual disassembly time and the HRC disassembly time.

Using disassembly parameters, human–robot collaborative disassembly time is derived from the operational time estimates from connector specifications. We can use a user-friendly spreadsheet to calculate disassembly time. Within this spreadsheet, individual rows represent different connectors, and their arrangement determines the disassembly sequence under evaluation. The ease of disassembly time metric requires three parts: disassembly information, disassembly parameters, and individual humans' and robots' disassembly time (Fig. 5).

Disassembly information consists of four segments provided by product designers. First, the product description defines information about components and connectors. The subsequent manual disassembly description details connector visibility, tools required, positioning, manipulation techniques, and component removal procedures. The robot disassembly factors evaluate the feasibility of robotic disassembly for connectors considering the five factors discussed in disassembly scores.

Finally, the robot disassembly description provides the specifics of robotic disassembly, including task types, tools employed, positioning considerations, fixture manipulation, grasping techniques, and methods for component removal.

The parameters used to calculate disassembly time are derived from various sources of disassembly information, including product descriptions and manual details. It incorporates both calculated time parameters and robotic disassembly factor parameters. Manual disassembly time parameters are computed using the Maynard Operation Sequence Technique (MOST) [8], and the robotic disassembly time is calculated through experiments. For robotic disassembly parameters, the calculation incorporates a 50% maximum robot speed assumption based on a robot's maximum Cartesian speed of 10 m/s, accounting for trapezoidal motion profiles and short distances during disassembly. Fixed

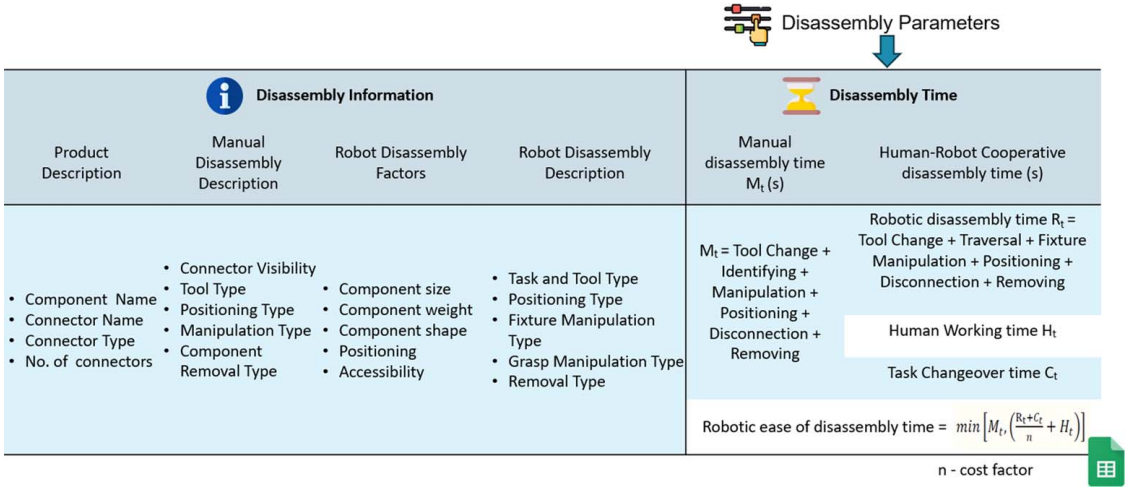

Fig. 5 Human–robot collaborative disassembly time metric

action times of 5 s are assumed for tool changing, grasping, and precise positioning and 2.5 s for task handover.

The parameters for the robotic disassembly factor take into account the disassembly scores. It is worth noting that disassembly parameters are calculated parameters, not measured parameters. As the robotic setup might vary for different applications, a generic robotic setup parameter is assumed for the metric, which aids in evaluating the product design irrespective of the human–robot collaborative setup design. The remanufacturers could revise these parameters depending on their setup to obtain a more accurate disassembly time for task planning and scheduling.

To determine whether to select manual disassembly or HRC, we need to calculate manual disassembly time (M_t) and human–robot collaborative time. Manual disassembly time (M_t) is calculated using

$$M_t = \text{tool change} + \text{identifying} + \text{manipulation} + \text{positioning} + \text{disconnection} + \text{removing} \quad (2)$$

The R_t is the robotic disassembly time calculated using

$$R_t = \text{tool change} + \text{traversal} + \text{fixture manipulation} + \text{positioning} + \text{disconnection} + \text{removing} \quad (3)$$

Thus, human–robot collaborative time is calculated using the equation below:

$$\text{Human–robot collaboartive time} = \left(\frac{R_t + C_t}{n} + H_t\right) \quad (4)$$

C_t is the task handover time determined by counting task transitions between humans and robots.

n is the cost factor, and it is determined based on parameters such as robot usage cost, availability, and labor cost (e.g., $n = 2$, assuming the robot incurs half the labor cost).

If a task is executable by a human and a robot, the metric attributes it to the robot, calculating the remaining tasks as human working time (H_t). The final disassembly time is computed as the minimum time between manual and human–robot collaborative disassembly. The disassembly time metric could be utilized to obtain feedback on the design and to iteratively improve the product design by identifying design challenges, dealing with different disassembly sequences, and meeting targets set by manufacturers or policymakers. The metric would benefit product designers in crafting circular designs, assist policymakers in assessing product circularity, and aid remanufacturers in disassembly task scheduling and allocation.

3 Case Study

3.1 XPS 8700 Desktop. This study used an XPS 8700 desktop computer as a case study to show the application of the proposed disassembly score. Figure 6 and Table 4 show the images and the list of components, including the power supply, HDD, CD reader, and other electronic devices. The desktop has two memory RAMs that were disassembled. Figure 7 shows the precedence relationships among the components, where the number in each cycle corresponds to the entries in Table 4. The figure differentiates between two types of lines: those without arrows indicate components at the same level of disassembly sequence, whereas lines with arrows show that certain components should be removed before proceeding to the next component. We excluded the side cover and the base as they are too large for the robotic gripper's capacity.

3.2 Components Used for Classification by MaxViT. Seven components were selected for analysis using the MaxViT model to identify component sizes. These components include a CD reader, HDD, CPU chip, GPU card, CPU fan, front cover, and power supply. Classification results show that the GPU card and HDD are considered small size; the CD reader and CPU chip are medium size; the CPU fan and front cover are large size; and the power supply is oversized. The camera was positioned at an equal distance for each component.

Moreover, we have collected 130 RGB images, which were manually labeled and resulted in 209 segmented images, as some examples are shown in Fig. 8. These segmented images were divided into training, validation, and testing datasets, with a ratio of 70%, 15%,

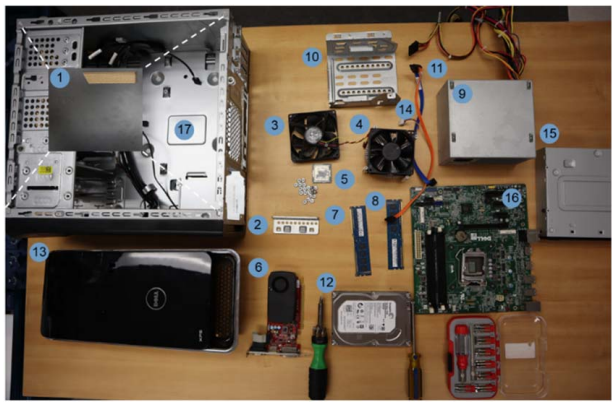

Fig. 6 The components of the XPS 8700 desktop

Table 4 The list of the components of XPS 8700

#	Component	#	Component	#	Component
1	Side cover	7	1st RAM	13	Front cover
2	Port cover	8	2nd RAM	14	Orange cable
3	Side fan	9	Power supply	15	CD reader
4	CPU fan	10	HDD cover	16	Motherboard
5	CPU chip	11	Blue cable	17	Base
6	GPU card	12	HDD		

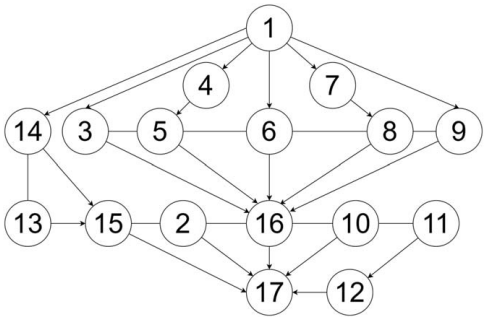

Fig. 7 The precedence relationships of XPS 8700 disassembly tasks

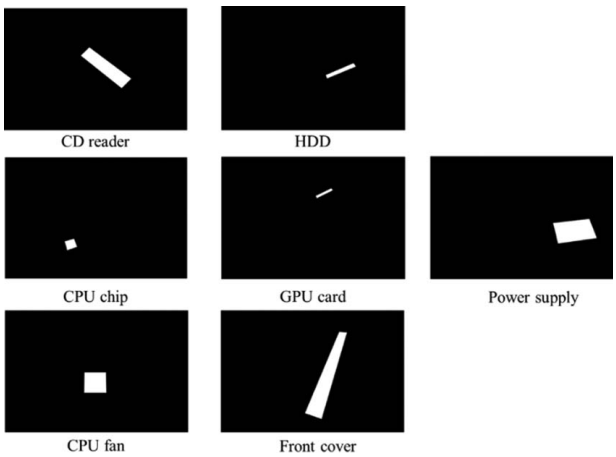

Fig. 8 Segmented images of seven components: CD reader, HDD, CPU chip, GPU card, CPU fan, front cover, and power supply

and 15%, respectively. The dataset consists of 130 RGB images captured using a high-resolution camera, with each image having dimensions of 6000 × 4000 pixels. These images were taken from various disassembly units of the XPS 8700 desktop, with each image shot at random angles to mimic real-world scenarios where a human worker might place objects in unpredictable positions. We used a desktop computer equipped with an i9-10900 K CPU @ 3.70 GHz, an NVIDIA Quadro RTX 4000 GPU, and 64 GB of RAM to train the machine-learning model. Data augmentation techniques were used on the training dataset before training the MaxViT model. Data augmentation improves the training dataset through random rerotations, horizontal flipping, and vertical flipping of images. This technique expanded the dataset and also simulated various real-world environments. Data augmentation was not applied to the testing dataset to assess the trained model's performance. This approach provides a solid evaluation of the model against an accurate representation of real-world data.

This study manually labels image segmentations, as shown in Fig. 8, and uses these segmented images as inputs to the MaxVit model for classifying component sizes. Although manual segmentation requires extra preprocessing, it increases accuracy by creating precise boundaries, improving training data quality, and reducing background noise. This method also benchmarks automated segmentation, reduces overfitting, and is helpful for high-precision tasks such as medical imaging and component analysis. In practice, RGB (Red-Green-Blue) images can be directly input into the classification model or first processed by a segmentation model to create segmented images for MaxVit to identify size classifications. While training a single object detection model may be simpler, a separate segmentation model offers valuable benefits despite the added complexity.

4 Results and Discussion

This section presents the disassembly score calculated for the XPS 8700 desktop, along with the application of the MaxViT machine-learning model for classifying component sizes and disassembly time calculation.

4.1 Disassembly Score for the XPS 8700 Desktop. The disassembly score is calculated for each component of the XPS 8700 desktop. Table 5 lists the characteristics of each component in terms of five factors: size, weight, shape, positioning, and accessibility. The shape of the component is quantified using Eq. (1), while positioning shows the component's order of rotational symmetry. Based on the data in Table 5, Table 6 shows the corresponding score for each factor. Most of the components are small in size and lightweight. The CPU chip and CD reader are categorized as medium sized, whereas the CPU fan and front cover are large. The power supply and motherboard are considered oversized, as their sizes exceed the maximum gripper opening of 8.5 cm. The blue and orange cables are considered asymmetric due to their variable shapes.

Regarding positioning, most components have an even order of rotational symmetry and are more accessible for the robot to handle. However, cables and the front cover are challenging to manipulate since their order of rotational symmetry is 1. Accessibility is limited for most components due to tight integration with the desktop casing or restricted space. The GPU card and two cables have medium accessibility, while the second RAM slot has sufficient space for the robotic gripper to navigate inside the desktop shell.

Table 7 shows the robotic capabilities for grasping and placing components. The grasping scores are calculated from the cumulative values of component size, weight, and shape, and the placing scores are calculated from the aggregation of positioning and accessibility. Due to oversized dimensions, the power supply and motherboard need manual disassembly. Most components have high grasping capability due to their lightweight and favorable shape; however, they have low placing capability.

This limitation in placing capability is because of the limited space available, as listed in Tables 5 and 6, which results in most components being classified under Semi-HRC conditions. This classification means the worker should position the component precisely before the robot grasps it and places it into the collection bin. The GPU card and second RAM have a high capability for grasping and placing, where the robotic gripper can access and manipulate these components inside the desktop. The robotic arm can work with the worker concurrently under the HRC setting.

In practice, when using the proposed disassembly scoring framework, it is important to assess the robotic limitations as detailed in the manual before integrating capabilities into the criteria, such as component weight and shape, as illustrated in Table 2. The evaluations for Grasping and Placing include factors such as component size, weight, shape, positioning, and accessibility, as shown in Table 3. The median score is the threshold for determining whether the robot can disassemble the objects. Table 6 presents the experimental results, which are then categorized according to the five different criteria from Table 2.

We acknowledge that the current application of the proposed framework is limited to a two-fingered simple gripper, which is

Table 5 The information of five factors for each component of the XPS 8700 desktop

Component	Size (cm)	Weight (g)	Shape (ref. symmetry)	Positioning (rot. symmetry)	Accessibility
Port cover	8.8 × 0.4 × 1	15	1	2	No space
Side fan	9.2 × 9.2 × 1.5	75	1	4	No space
CPU fan	8 × 8 × 6	365	1	4	No space
CPU chip	3.8 × 3.8 × 0.4	25	1	4	No space
GPU card	5.5 × 9.6 × 1.5	140	1	2	Need to remove the CPU fan
1st RAM	3 × 13.5 × 0.1	10	1	2	Need to remove the GPU card and 1st RAM
2nd RAM	3 × 13.5 × 0.1	10	1	2	High Accessibility
Power supply	14 × 15 × 8.6	1540	1	2	No space
HDD cover	11 × 13.7 × 0.1	135	1	2	No space
Blue cable	26.5 × 0.8 × 0.3	5	<0.5	1	Medium Accessibility
HDD	11 × 14.6 × 2	390	1	2	No space
Front cover	5 × 18 × 41	570	1	1	No space
Orange cable	36.5 × 0.8 × 0.3	5	<0.5	1	Medium Accessibility
CD reader	14.6 × 17 × 4.1	645	1	2	No space
Motherboard	22.2 × 24 × 0.4	460	1	2	No space

Table 6 The resulting score for each factor

Component	Size	Weight	Shape	Positioning	Accessibility
Port cover	Small (1)	Light (5)	Symmetric (5)	Easy (5)	Low (1)
Side fan	Small (1)	Light (5)	Symmetric (5)	Easy (5)	Low (1)
CPU fan	Large (5)	Light (5)	Symmetric (5)	Easy (5)	Low (1)
CPU chip	Medium (3)	Light (5)	Symmetric (5)	Easy (5)	Low (1)
GPU card	Small (1)	Light (5)	Symmetric (5)	Easy (5)	Medium (3)
1st RAM	Small (1)	Light (5)	Symmetric (5)	Easy (5)	Low (1)
2nd RAM	Small (1)	Light (5)	Symmetric (5)	Easy (5)	High (5)
Power supply	X	Light (5)	Symmetric (5)	Easy (5)	Low (1)
HDD cover	Small (1)	Light (5)	Symmetric (5)	Easy (5)	Low (1)
Blue cable	Small (1)	Light (5)	Asymmetric (1)	Difficult (1)	Medium (3)
HDD	Small (1)	Light (5)	Symmetric (5)	Easy (5)	Low (1)
Front cover	Large (5)	Light (5)	Symmetric (5)	Difficult (1)	Low (1)
Orange cable	Small (1)	Light (5)	Asymmetric (1)	Difficult (1)	Medium (3)
CD reader	Medium (3)	Light (5)	Symmetric (5)	Easy (5)	Low (1)
Motherboard	X	Light (5)	Symmetric (5)	Easy (5)	Low (1)

Table 7 The work settings based on disassembly factors and robotic capability

Component	Grasping	Placing	Grasping capability	Placing capability	Work collaboration ability
Port cover	11	6	High	Low	Semi-HRC
Side fan	11	6	High	Low	Semi-HRC
CPU fan	15	6	High	Low	Semi-HRC
CPU chip	13	6	High	Low	Semi-HRC
GPU card	11	8	High	High	HRC
1st RAM	11	6	High	Low	Semi-HRC
2nd RAM	11	10	High	High	HRC
Power supply	X	X	X	X	Worker-Only
HDD cover	11	6	High	Low	Semi-HRC
Blue cable	7	4	Low	Low	Worker-Only
HDD	11	6	High	Low	Semi-HRC
Front cover	15	2	High	Low	Semi-HRC
Orange cable	7	4	Low	Low	Worker-Only
CD reader	13	6	High	Low	Semi-HRC
Motherboard	X	X	X	X	Worker-Only

designed to handle specific shapes, sizes, and weights. The primary constraint is the gripper's opening width combined with the payload capacity of the robotic arm. Despite these limitations, this type of gripper is common in practice due to its cost-effectiveness, ease of implementation, and suitability for common disassembly tasks such as pick-and-place operations. Thus, we chose UR5e with a two-fingered gripper to emphasize essential disassembly factors rather than incorporating the complexities of advanced grippers. This study specifically addresses the sensitivity of disassembly to the physical attributes of objects, such as the gripper's capacity to handle the weight, the robotic arm's ability to support this weight, and the adequacy of space for the gripper and robotic arm to access the object in constrained environments. Despite its limitations, the proposed disassembly scoring framework can be applied to other gripper designs, and the methodology can be expanded to include alternative gripper types, such as vacuum or multifinger grippers.

4.2 Component Size Classification Results. To demonstrate how machine learning can identify disassembly factors such as component size with computer vision, we utilized the MaxViT architecture. The MaxViT classifies component sizes into four categories: small, medium, large, and oversize, which are assigned labels 1, 2, 3, and 4, respectively.

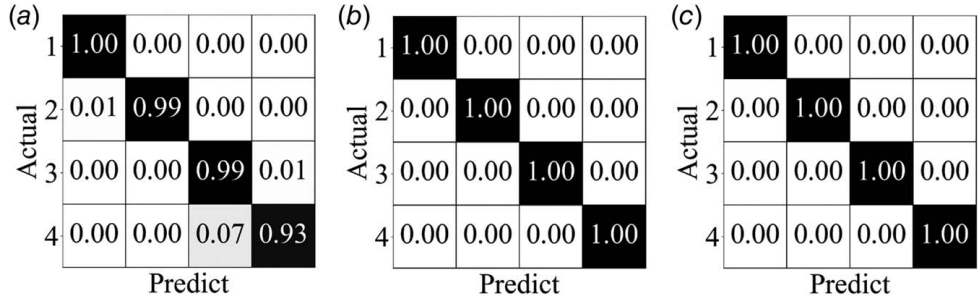

Fig. 9 The normalized confusion matrix of (*a*) training results with 98% accuracy, (*b*) validation results with 100% accuracy, and (*c*) testing results with 100% accuracy

Figure 9 shows the normalized confusion matrix results of training, validation, and testing datasets. The training accuracy is 98%, while the validation and testing accuracy is 100%. The MaxViT model can classify the component size perfectly. In the training phase shown in Fig. 9(*a*), the sizes, such as medium, large, and oversize, lost some accuracy, which the MaxViT classed into the nearby size. For example, in oversize (4), 7% of images are classed into large sizes, and others, such as small and medium, do not have misclassification. This shows the capabilities of using machine learning to identify disassembly factors toward an automated rating system. While simpler classification algorithms could be employed in this case, we chose MaxViT to demonstrate a machine-learning model that is capable of handling more complex scenarios. This provides flexibility for future cases in which the classification task may include more challenging component characteristics.

In this study, we do not consider summing the pixels in segments. While summing pixels can indicate the area of a component, it does not reflect whether the robot can grasp it. For instance, two objects —one measuring 90 mm × 90 mm and another 30 mm × 270 mm— have the same area, but the robot cannot grasp the first one due to its 85-mm limitation. In this study, we used the MaxViT model exclusively to classify component sizes by demonstrating its near-perfect efficacy in size identification. The MaxViT's robust performance in classification tasks makes it a suitable architecture in this example. For future research, an alternative approach could include using an object detection model such as YOLO, which would categorize sizes and provide bounding boxes to determine the precise dimensions of objects.

The MaxViT model demonstrates an example of classification with automated size assessment. This example suggests that future studies could develop an automated rating system for disassembly scores based on the MaxViT model, even with unknown size information. The deep learning model requires only the image as input and then evaluates the disassembly scores automatically.

Although the real-time application was beyond the scope of this study, which introduced a new scoring system from the perspective of robotic capabilities for optimal work settings, future research could expand to include real-time computer vision applications. The performance of the vision system may be affected by environmental variables such as lighting conditions and occlusions, which affect the system's accuracy. In the current study, we used high-resolution images captured under ideal conditions, where we obtained nearly perfect results. Future research could address challenges associated with real-time operations, such as noise introduced by the movement of human hands and robotic arms, which can significantly impact the performance of the vision system in dynamic environments.

4.3 Calculation of Disassembly Time for the XPS 8700 Desktop. Considering the robot's capabilities and the design of the case study product especially low placing capability due to the limited space available, most of the tasks are carried out by manual disassembly. Considering the human–robot collaborative disassembly time calculation, the total manual disassembly time (M_t) for the XPS 8700 desktop was found to be 145.8 s. Factoring in robotic capabilities, the robotic disassembly time (R_t) was 60.82 s, with the remaining tasks accounting for human working time (H_t) at 128.16 s and a task changeover time (C_t) of 37.5 s. Considering a cost factor (n) of 2, the final disassembly time was calculated as 145.8 s. We should note that the obtained disassembly time is based on the calculated disassembly parameters for uniformity of the product design evaluation. Hence, the computed disassembly time values will differ from the actual measured disassembly times in practice.

The manual disassembly time was determined using the MOST, a standardized predetermined motion time system. In this approach, the disassembly task was broken down into individual motion elements (e.g., reach, grasp, move), each assigned a numerical time value based on established standards. Although the manual disassembly time was not measured directly by users performing the task, the MOST methodology naturally accounts for human variability through its standardized time data, derived from extensive empirical studies.

While the disassembly scores define each component's work setting, the disassembly time reflects the overall productivity of the XPS 8700 desktop dismantling. This metric can inform product design improvements to make disassembly more HRC-friendly by optimizing connectors for quicker, more practical disassembly that robots can easily handle. Future research could leverage disassembly scores and time metrics to evaluate and compare various design alternatives.

4.4 Practical Implications and Limitations. This study can be reproduced by focusing on two main factors: (1) the disassembly objects and (2) the selected robot. Component weight and size should match the robot's maximum payload and the gripper's capacity when using the scores developed in this study. Component shape and positioning should be evaluated using the criteria from Table 2. Experiments are needed to check if there is enough space for the robotic arm to operate properly.

Using the right types of grippers and robotic arms is important as described in Table 2. The success of repeating the disassembly process depends mainly on the robot's hardware and its control system. Factors such as position errors, overshooting, and gripper failures can affect how well the robot handles and manipulates components, especially those oddly shaped or hard to access. Misalignments caused by the robot's movements might lead to gripping and arm movement failures.

This study did not include a detailed sensitivity analysis, but future work will investigate how these variations influence the framework's effectiveness. When applied to different types of hardware, the performance of the proposed framework may vary based on various configurations and environmental conditions. For example, using advanced grippers such as vacuum or multifinger types can improve handling irregular shapes and oversized components. Moreover, robots with higher payloads typically show improved repeatability and accuracy. Environmental factors such as lighting, workspace, and noise can also affect robotic performance in vision-based tasks, as these elements are important to the robotic control system and hardware requirements. For

experimental replications, consistent results are expected under controlled conditions. However, variations might occur due to mechanical wear, calibration drift, or slight differences in component placement. Future studies could include repeated trials for various hardware setups to analyze the impact of different environmental conditions.

5 Conclusion

This study proposes a framework for assessing the disassembly score suitable for robotic disassembly based on five factors: component size, weight, shape, positioning, and accessibility. It discusses the connection between disassembly factors, robotic capabilities, and workplace settings. The application of the proposed disassembly scoring framework is shown by using an XPS 8700 desktop. Moreover, the study uses MaxViT, a transformer-based machine-learning model, to categorize component sizes into four classes: small, medium, large, and oversized. The framework provides a rating system for determining the ease of robots performing disassembly tasks. Further, using MaxViT proves that artificial intelligence techniques can be used to automate the development of scoring systems. This is particularly important in remanufacturing sites, where various products with different models, conditions, and types are received. AI can quickly assess and sort these products based on their characteristics. The study also provided a framework for comparing manual disassembly time with human–robot disassembly time as the base for decision-making and determining a practical disassembly work setting.

The study can be extended in several ways. The future automated rating systems can be further developed. It will be easier for robots to evaluate the ease of disassembly and handling of each component by using computer vision techniques. Moreover, other robotic grippers, such as vacuum and humanoid hand grippers, can be used beyond just the two-finger gripper. The analysis mainly considers the robotic perspective and neglects the human worker's viewpoint. In addition, the research could be expanded to include other deep learning models such as GoogLeNet and U-Net to further compare their performance in identifying vision-based factors. Currently, the study focuses mainly on the proposed disassembly scores and the calculation of disassembly time with respect to product design and robotic capabilities. Further research is needed for real-world evaluation, to determine the best computer vision model suitable for real-time settings, and to conduct model comparisons. Future research could broaden the disassembly scoring framework to include robotic and human considerations, such as human factors and fatigue. Also, the use of a disassembly score can be shown in the product design phase to facilitate designing products that are easier for robots to disassemble.

Acknowledgment

This material is based upon work supported by the National Science Foundation-USA under Grant No. 2026276. Any opinions, findings, conclusions, or recommendations expressed in this material are those of the authors and do not necessarily reflect the views of the National Science Foundation.

Conflict of Interest

There are no conflicts of interest.

Data Availability Statement

The datasets generated and supporting the findings of this article are obtainable from the corresponding author upon reasonable request.

References

[1] Hjorth, S., and Chrysostomou, D., 2022, "Human–Robot Collaboration in Industrial Environments: A Literature Review on Non-Destructive Disassembly," Rob. Comput. Integr. Manuf., **73**, p. 102208.
[2] Liao, H.-Y., Chen, Y., Hu, B., and Behdad, S., 2023, "Optimization-Based Disassembly Sequence Planning Under Uncertainty for Human–Robot Collaboration," ASME J. Mech. Des., **145**(2), p. 022001.
[3] Al Handawi, K., Andersson, P., Panarotto, M., Isaksson, O., and Kokkolaras, M., 2021, "Scalable Set-Based Design Optimization and Remanufacturing for Meeting Changing Requirements," ASME J. Mech. Des., **143**(2), p. 021702.
[4] Nemani, V. P., Liu, J., Ahmed, N., Cartwright, A., Kremer, G. E., and Hu, C., 2022, "Reliability-Informed Economic and Energy Evaluation for Bi-Level Design for Remanufacturing: A Case Study of Transmission and Hydraulic Manifold," ASME J. Mech. Des., **144**(8), p. 082001.
[5] Behtash, M., Liu, X., Davied, M., Thompson, T., Burjes, R., Lee, M., Wang, P., and Hu, C., 2024, "Reman Co-Design: A Combined Design and Remanufacturing Optimization Framework for the Sustainable Design of High-Value Components," ASME J. Mech. Des., **146**(2), p. 020901.
[6] Kim, J., Park, S., and Kim, H. M., 2022, "Optimal Modular Remanufactured Product Configuration and Harvesting Planning for End-of-Life Products," ASME J. Mech. Des., **144**(4), p. 042001.
[7] Desai, A., and Mital, A., 2003, "Evaluation of Disassemblability to Enable Design for Disassembly in Mass Production," Int. J. Ind. Ergon., **32**(4), pp. 265–281.
[8] Vanegas, P., Peeters, J. R., Cattrysse, D., Tecchio, P., Ardente, F., Mathieux, F., Dewulf, W., and Duflou, J. R., 2018, "Ease of Disassembly of Products to Support Circular Economy Strategies," Resour. Conserv. Recycl., **135**, pp. 323–334.
[9] IFixit, 2025, https://www.ifixit.com/repairability/smartphone-repairability-scores
[10] Bracquené, E., Peeters, J., Alfieri, F., Sanfélix, J., Duflou, J., Dewulf, W., and Cordella, M., 2021, "Analysis of Evaluation Systems for Product Repairability: A Case Study for Washing Machines," J. Cleaner Prod., **281**, p. 125122.
[11] Mummolo, G., Bari, P., Menolascina, F., Elettrotecnica, I., Orabona, V., Salento, U., Siena, G. P., Ospedale, I., and Sollievo, C., 2007, "A Fuzzy Approach for Medical Equipment Replacement Planning," Third International Conference on Maintenance and Facility Management, pp. 229–235.
[12] Peeters, J. R., Tecchio, P., Ardente, F., Vanegas, P., Coughlan, D., and Duflou, J. R., 2018, *eDIM: Further Development of the Method to Assess the Ease of Disassembly and Reassembly of Products: Application to Notebook Computers*, Publications Office of the European Union, Luxembourg.
[13] Zhu, W., Fan, X., and He, Q., 2020, "A Hierarchical and Process-Oriented Framework for Disassemblability Evaluation in Product Maintainability Design," Int. J. Adv. Manuf. Technol., **110**(3–4), pp. 777–795.
[14] De Fazio, F., Bakker, C., Flipsen, B., and Balkenende, R., 2021, "The Disassembly Map: A New Method to Enhance Design for Product Repairability," J. Cleaner Prod., **320**, p. 128552.
[15] Qiu, L., Liu, X., Zhang, S., and Sun, L., 2014, "Disassemblability Modeling Technology of Configurable Product Based on Disassembly Constraint Relation Weighted Design Structure Matrix (DSM)," Chin. J. Mech. Eng., **27**(3), pp. 511–519.
[16] Yadav, D. P., Patel, D. N., and Morkos, B. W., 2018, "Development of Product Recyclability Index Utilizing Design for Assembly and Disassembly Principles," ASME J. Manuf. Sci. Eng., **140**(3), p. 031015.
[17] Germani, M., Mandolini, M., Marconi, M., and Rossi, M., 2014, "An Approach to Analytically Evaluate the Product Disassemblability During the Design Process," Procedia CIRP, **21**, pp. 336–341.
[18] Go, T. F., Wahab, D. A., Rahman, M. N. A., Ramli, R., and Azhari, C. H., 2011, "Disassemblability of End-of-Life Vehicle: A Critical Review of Evaluation Methods," J. Cleaner Prod., **19**(13), pp. 1536–1546.
[19] Sawanishi, H., Torihara, K., and Mishima, N., 2015, "A Study on Disassemblability and Feasibility of Component Reuse of Mobile Phones," Procedia CIRP, **26**, pp. 740–745.
[20] Parsa, S., and Saadat, M., 2019, "Intelligent Selective Disassembly Planning Based on Disassemblability Characteristics of Product Components," Int. J. Adv. Manuf. Technol., **104**(5), pp. 1769–1783.
[21] Ali, A., Enyoghasi, C., and Badurdeen, F., 2022, "A Quantitative Approach forProduct Disassemblability Assessment," *Role of Circular Economy in Resource Sustainability*, P. Ghadimi, M. D. Gilchrist, and M. Xu, eds., Springer Cham, Cham, Switzerland, pp. 73–84.
[22] Li, K., Liu, Q., Xu, W., Liu, J., Zhou, Z., and Feng, H., 2019, "Sequence Planning Considering Human Fatigue for Human-Robot Collaboration in Disassembly," Procedia CIRP, **83**, pp. 95–104.
[23] Vongbunyong, S., Kara, S., and Pagnucco, M., 2013, "Basic Behaviour Control of the Vision-Based Cognitive Robotic Disassembly Automation," Assem. Autom., **33**(1), pp. 38–56.
[24] Parsa, S., and Saadat, M., 2021, "Human-Robot Collaboration Disassembly Planning for End-of-Life Product Disassembly Process," Rob. Comput. Integr. Manuf., **71**, p. 102170.
[25] Hu, H., Liu, Y., Lu, W. F., and Guo, X., 2022, "A Quantitative Aesthetic Measurement Method for Product Appearance Design," Adv. Eng. Inform., **53**, p. 101644.
[26] Steinhardt, P., 2019, *The Second Kind of Impossible: The Extraordinary Quest for a New Form of Matter*, Simon and Schuster, New York.
[27] Tu, Z., Talebi, H., Zhang, H., Yang, F., Milanfar, P., Bovik, A., and Li, Y., 2022, "Maxvit: Multi-Axis Vision Transformer," European Conference on Computer Vision, Tel Aviv, Israel, Oct. 23–27, pp. 459–479.
[28] Sandler, M., Howard, A., Zhu, M., Zhmoginov, A., and Chen, L.-C., 2018, "Mobilenetv2: Inverted Residuals and Linear Bottlenecks," Proceedings of the IEEE Conference on Computer Vision and Pattern Recognition, Salt Lake City, UT, June 18–23, pp. 4510–4520.